Materials Express

2158-5849/2019/9/851/010
doi:10.1166/mex.2019.1584
www.aspbs.com/mex

Evaluating weld properties of conventional and swept friction stir spot welded 6061-T6 aluminium alloy

S. Suresh[1], K. Venkatesan[2,*], Elango Natarajan[3,*], S. Rajesh[4], and Wei Hong Lim[3]

[1]*Department of Mechanical Engineering, Jayalakshmi Institute of Technology, 636352, India*
[2]*Department of Metallurgical Engineering, Government College of Engineering, Salem 636011, India*
[3]*Faculty of Engineering, UCSI University, Kuala Lumpur, 56000, Malaysia*
[4]*Department of Mechanical Engineering, Knowledge Institute of Technology, Salem 637504, India*

ABSTRACT

6061-T6 aluminium alloy is a tempered grade aluminium material that is extensively used, particularly in space and automotive applications. The conventional and swept friction stir spot welding (FSSW) joints are prepared by varying tool rotational speed at four different levels. The mechanical properties, microstructure and mode of failure in both types of FSSW are evaluated and reported. The high plastic deformation and fine grains influenced the increase in hardness of the weld joints based on the Hall-Petch equation. The highest lap shear strength of 5.31 kN is observed in swept FSSW sample prepared at 1400 rpm. Interestingly, 1600 rpm decreased the lap shear strength due to insufficient friction between base metal and tool in the higher tool rotational speed. The minimum microhardness is noticed in heat-affected zone (HAZ) of both cases. Conventional FSSW samples showed shear fracture, nugget pullout fracture and circumferential fracture under lap shear loading, whereas swept FSSW showed only the circumferential fracture.

Keywords: FSSW, HAZ, Aluminium Alloy, Hall-Petch, Swept FSSW, Lap Shear Strength.

1. INTRODUCTION

In recent years, the use of aluminium alloys has increased in space frame structures, and inner and outer panels of automobiles in view of improving the sustainability of the industries [1–3]. 6061-T6 aluminium alloy is a tempered grade aluminium alloy which has good mechanical properties than others. It has been used in aircraft, automobiles, marines, and even bicycles. Since 2003, Friction Stir Spot Welding (FSSW) developed by Mazda Motor Corp has proven to be an impending applicant for spot welding low weight alloys, principally in fastening the door panels in automobile assemblies [4]. FSSW might reduce the energy consumption by 90%, improve joint performance and the installation cost by 40%, compared to Resistance Spot Welding (RSW) [5]. In addition, it has more benefits in the aspect of metallurgical, environmental and energy consumption over other joining methods [6–7]. FSSW creates a spot weld in a distinct location through plunging, stirring and retracting actions. The conventional FSSW, swept FSSW and refilled FSSW are three different versions in FSSW. Each of these FSSW processes has different level of complexity and diversity in terms of spot shear area, shear strength, the degree of control in motion and time to complete the weld [8].

In the conventional FSSW, a single piece of non-consumable rotating FSSW tool is initially plunged into the base material and held in place for a certain period. The tool is then retracted that leads to producing a localised joint in the base material around the tool pin. In Swept

*Authors to whom correspondence should be addressed.
Emails: venkisree@yahoo.com, cad.elango.n@gmail.com

Article

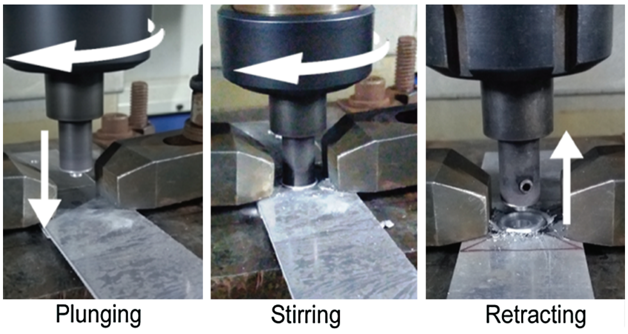

Fig. 1. Different stages of conventional FSSW process.

FSSW, the tool is plunged and moved additionally in a circular path. Both these techniques leave a circular indentation on the top side of the joint (exit hole) which is same as tool pin diameter. Refill FSSW eliminates the form of exit hole as the tool comprises an external clamp, pin and a shoulder with the separate drive mechanism.

The various stages of conventional and swept FSSW processes are shown in Figures 1 and 2. Many researchers implemented the conventional FSSW on aluminium alloys, especially AA6061 and investigated the importance of various welding parameters on the joint strength, fracture surfaces and tool configuration [9–13]. The tool rotational speed is a significant welding parameter in FSSW, followed by tool shoulder plunge depth and dwell time. The literature [14, 15] reported that the strength of the joint is highly influenced by the tool rotational speed. Okamoto et al. [16] conducted the stitch-FSW experiment on aluminium alloy, compared with the conventional FSSW and reported that the additional linear movement of the tool in stitch-FSW significantly increases the joint strength. A few researches were done on the influence of welding parameters on the weld properties of Swept FSSW process. Awang et al. [17] investigated the swept FSSW on aluminium alloy and reported that the tool travel speed is related with the heat dissipation that significantly influences the strength of the joint.

Brown et al. [18] studied the fatigue life and tensile strength of Swept-FSSW on the anodized AA2219-T6 sheet and reported that swept-FSSW has better tensile and fatigue strength as a rivet. Su et al. [19, 20] estimated the fatigue life of swept FSSW on the alclad 2024-T3 aluminium sheets and reported that the circular motion of tool affects the fatigue life of spot joints. Buffa et al. [21] conducted the FSSW experiments with different tool path and suggested that the circular path FSSW has more stirred area and joint strength. However, not enough studies have been done on a comparison of conventional and swept FSSW processes in terms of mechanical and metallurgical behaviour. In the present research, the weld properties of conventional and swept FSSW processes in a thin sheet of aluminium alloy 6061-T6 have been investigated and compared.

2. MATERIALS AND METHODS

2.1. Materials and Tool

The weld specimens of aluminium alloy 6061-T6 material (supplied by Cluster Trading Corporation, India) was prepared in the size of $100 \times 35 \times 2$ mm through Electrical Discharge Machining (EDM). Figure 3 shows the dimension of the overlap configuration of the lap shear test specimen. Table I shows the properties of aluminium alloy 6061-T6 base material.

H13 steel tool hardened to 52–55 HRC in the dimension of 12 mm shoulder diameter, 5 mm threaded cylindrical pin and 2.85 mm length was used as a tool. Figure 4 depicts the detail of FSSW tool used in the weld process.

2.2. Experimental Method

2.2.1. Preparation of FSSW Samples

The conventional FSSW and swept FSSW were conducted using a computer numerical control vertical machining center (ACE micrometric make) with a fixture to clamp the overlapping area of the sheets as shown in Figure 5. The weld parameters were chosen based on the preliminary studies and the existing literatures [8–13]. Four different tool rotational speed; typically as 900, 1200, 1400 and 1600 rpm were used in both cases. Other parameters such as plunge depth, tool travel speed and dwell

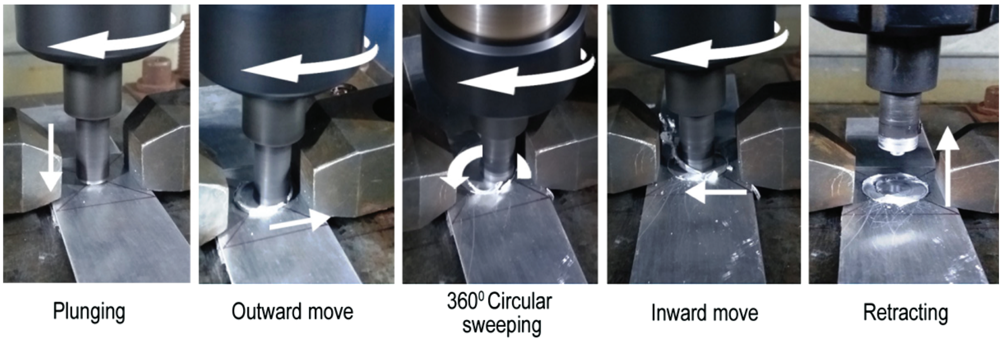

Fig. 2. Different stages of swept FSSW process.

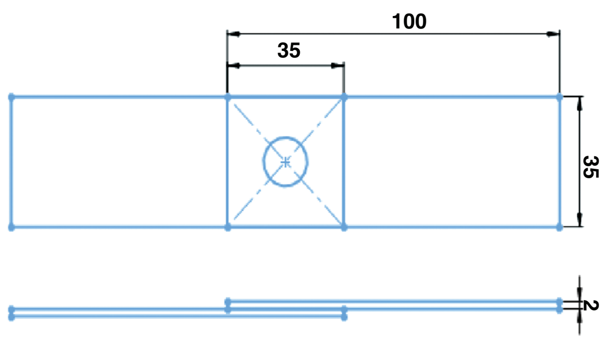

Fig. 3. Dimensions of the overlap configuration of FSSW specimen (all dimensions in mm).

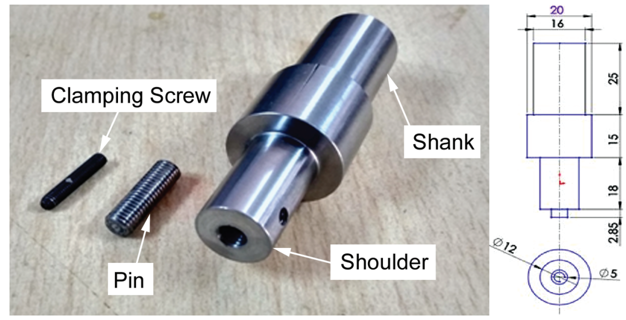

Fig. 4. Details of FSSW tool.

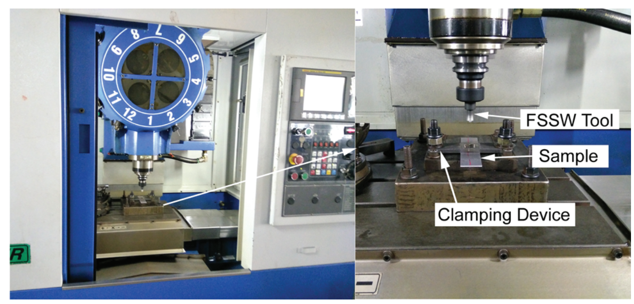

Fig. 5. FSSW experimental setup in CNC machine.

time were kept constant as 0.2 mm, 10 mm/minute and 5 seconds respectively for all the experiments, irrespective of the method used. During swept FSSW, the radius of circular interpolation of the tool after plunging was 2.5 mm. It is obvious that conventional FSSW does not have circular interpolation of the tool after plunging. The impurities in the overlapping surfaces of the plates were cleaned with acetone before welding. Three samples in each condition were prepared for the investigations.

2.2.2. Microhardness and Lap Shear Tests

Microhardness and lap shear strength of the welded joints were measured using Vicker's microhardness tester (Wilson hardness, 402 MVD, Wilson Instruments, Norwood) and computerized universal testing machine (TE-JINAN-WDW100, Jinan Test Machine Co. Ltd., China) respectively. The hardness profile was obtained for 1 kg of force for a dwell time of 20 seconds. The lap shear test was conducted at a crosshead speed of 1 mm/minute at room temperature and the lap shear strength of the weld was reported by averaging the results of three individual specimens in each welding condition.

2.2.3. Metallurgical Characterization

After the lap shear tests, the standard metallographic techniques were used for preparing the cross-sectioned samples. The Keller's reagent containing 5 ml HNO_3, 3 ml HCl, 2 ml HF, and 190 ml H_2O was used to reveal the microstructure of the weld cross-section. The macro and microstructural characterisation of the cross-section of the joints were investigated using stereo zoom microscope (Radical RSM-9, Radical Scientific, India) and optical microscope (Invertoplan TR, Gippon-Japan) respectively. Figure 6 shows the sample prepared for lap shear test and metallurgical examinations.

The fracture surfaces of the lap shear tested specimens were further analysed through Field Emission Scanning Electron Microscope (SIGMA HV-Carl Zeiss, Germany) to understand the failure mechanism.

3. RESULTS AND DISCUSSION

3.1. Visual Inspection

Figure 7 depicts the top view of the weld samples prepared from conventional and swept FSSW. Unlike conventional FSSW (Figs. 7(a–d)), the visual aspect of the welds made by swept FSSW (Figs. 7(e–h)) looks bigger in size due to the circular indentation of the shoulder at the top sheet.

In conventional FSSW, the squeezed out materials at the end of the plunging stage are accumulated around the circumference of the tool shoulder indentation. But in swept FSSW, the additional circular movement of the tool after plunging has significantly decreased the formation of the

Table I. Properties of 6061-T6 aluminium alloy.

Chemical composition (Wt.%)									Mechanical properties		
Mg	Si	Fe	Cu	Cr	Mn	Ti	Zn	Al	Ultimate tensile strength (MPa)	Hardness Vicker's (HV)	Elongation (%)
0.708	0.43	0.49	0.164	0.14	0.097	0.04	0.004	Rem	310	107	10

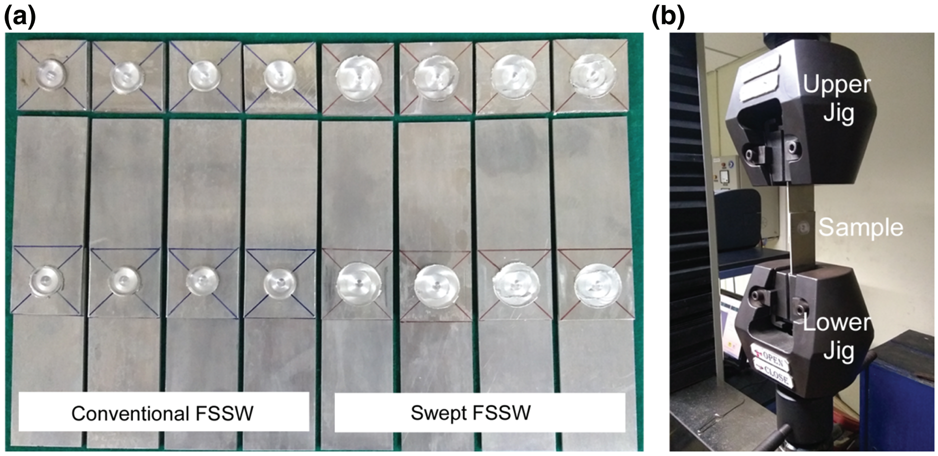

Fig. 6. (a) Samples prepared for the lap shear test and metallurgical investigation. (b) Photograph of lap shear test setup.

squeezed out material around the indentation in the top plate, which could be the reason for having the big size in swept FSSW samples. The surface defect was observed only from the sample of swept FSSW with the rotational speed of 1600 rpm (as shown in Fig. 7(h)). It could be resulted from the incomplete filling of stirred material around the keyhole.

3.2. Macro Examinations

Macro examination was carried out to present a cross-sectional structure of the joints and to detect internal flaws of the joints. Figure 8 shows the macrographic observations along the cut sectional plane of the spot welds, obtained from conventional FSSW with different tool rotation speed.

It is observed that all the samples are free from defects. The tool pin displaced the stirred material below the shoulder and around the pin. The hook was formed adjacent to the stirring area between the two sheets due to the vertical displacement of the faying surfaces. It is also worth to indicate that the width of the stir zone (SZ_W) varies with respect to the tool rotational speed. The distance between the widest region of the SZ and edge of the keyhole is considered to define the width of the SZ.

Figure 9 depicts the macrographic appearances along the cut sectional plane of the welds obtained through swept FSSW with the different tool rotating speed. Macrostructure of all the samples except joints of higher rotational speed of 1600 rpm shows defect-free surfaces due to good mixing. The tunneling/wormhole defect at the end of stir

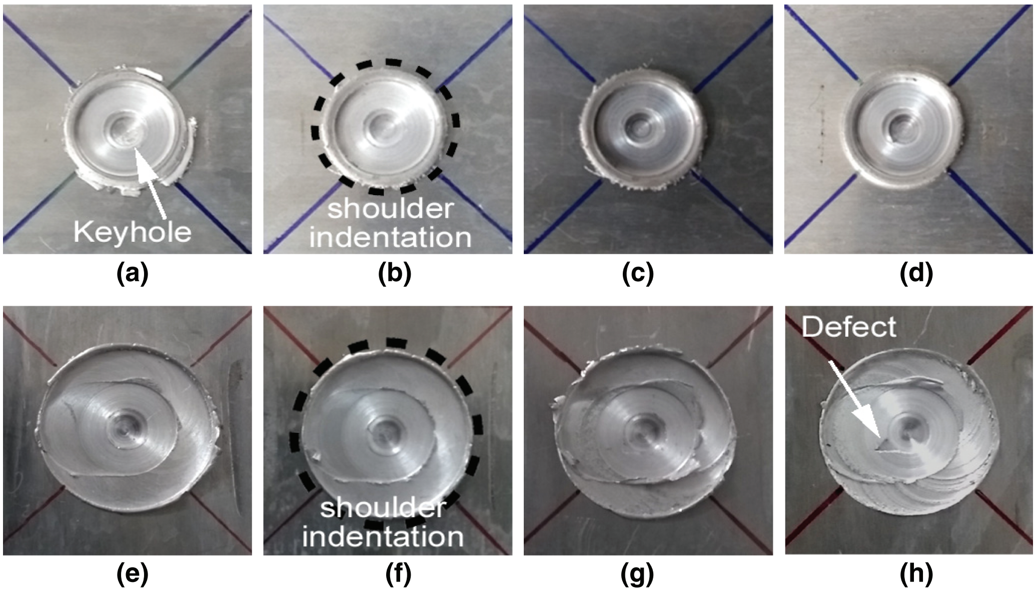

Fig. 7. Photograph of top view of weld (a–d) conventional FSSW (e–h) swept FSSW.

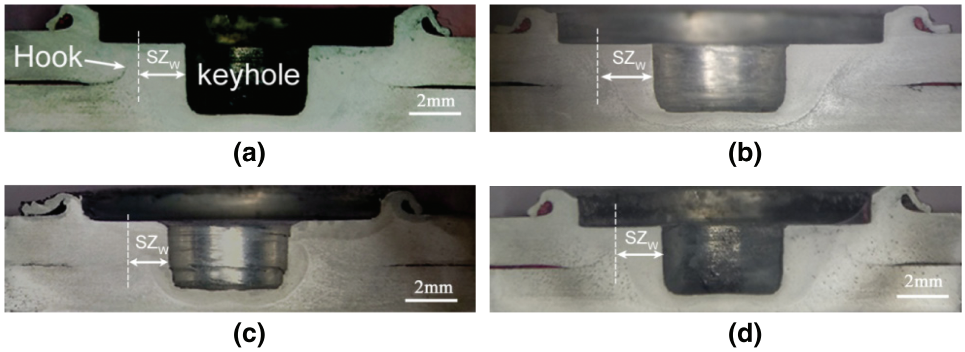

Fig. 8. Macro examination of conventional FSSW at 10× (a) 900 rpm (b) 1200 rpm (c) 1400 rpm and (d) 1600 rpm.

zone was observed at the rotational speed of 1600 rpm. The high tool rotational speed can increase the turbulence in the material flow and strain rate which could be the reason for a tunneling defect at the weld nugget which is similar to that reported by Awang et al. [22].

Two kinds of the material flow pattern were observed in the weld area of the cross-sectional profile of swept FSSW samples. The first pattern is on the stirred area around the keyhole (as represented as I in Fig. 9) due to the plunging sequence. The other pattern is away from the keyhole (as represented as II in Fig. 9) because of the circumferential action of the tool that leads to the horizontal material flow. But conventional FSSW showed only one pattern (Pattern I) on the stirred area around the keyhole. The swept FSSW has more stirred area and lesser formation of the hook which leads to an effective increase in joint strength than conventional FSSW.

3.3. Microhardness

The various zones of the weld cross-sections according to the characteristics are stir zone (SZ), thermo-mechanically affected zone (TMAZ), heat affected zone (HAZ), and base material (BM) [23, 24]. Figures 10 and 11 shows Vicker microhardness of conventional FSSW and swept FSSW samples respectively. The different zones of the weld; SZ, TMAZ and HAZ are considered to measure hardness value and to understand the variation. The microhardness was measured from the cross-section of weld centre of the samples in a spacing of 1 mm along parallel lines in the middle of the top plate and middle of the bottom plate. The microhardness distributions are nearly symmetric about the centre of the keyhole.

In both the conventional and swept FSSW joints, the SZ below and around the keyhole have higher hardness. The hardness decreases all the way through TMAZ and reaches a minimum value in the HAZ. It can be observed that the tool rotational speed has a little influence on the hardness variation in all the regions, irrespective of the methods used. The increase in microhardness value in SZ is observed in swept FSSW joint, compared with the conventional FSSW. This could be because of higher plastic deformation due to the additional stirring action of the tool [25]. The high plastic deformation and fine grains influenced the increase in the micrhardness of the SZ based on the Hall-Petch equation [9]. This is in agreement with the effect that is reported by Zhang et al. [26] and Venukumar et al. [13].

3.4. Lap Shear Tensile Strength

Figure 12 showed the comparison of lap shear strength between conventional and swept FSSW at the different tool rotational speeds. Swept FSSW joints show higher lap shear strength compared to conventional FSSW for all the tool rotational speeds, which looks good agreement with the observed hardness values. The increase in lap shear strength of swept FSSW joints is most likely because of

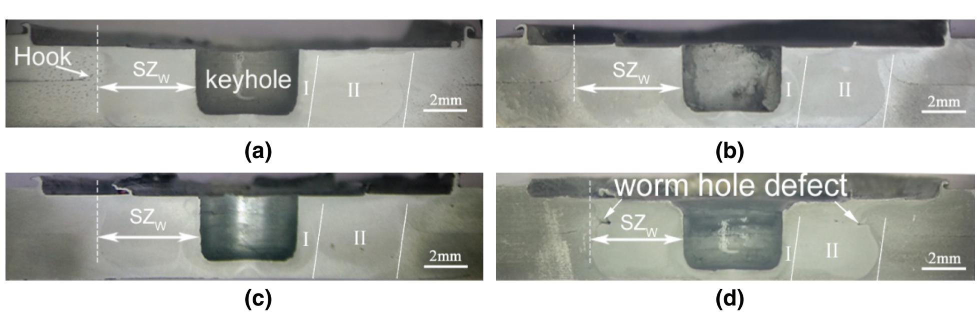

Fig. 9. Macro examination of swept FSSW at 10× (a) 900 rpm (b) 1200 rpm (c) 1400 rpm and (d) 1600 rpm.

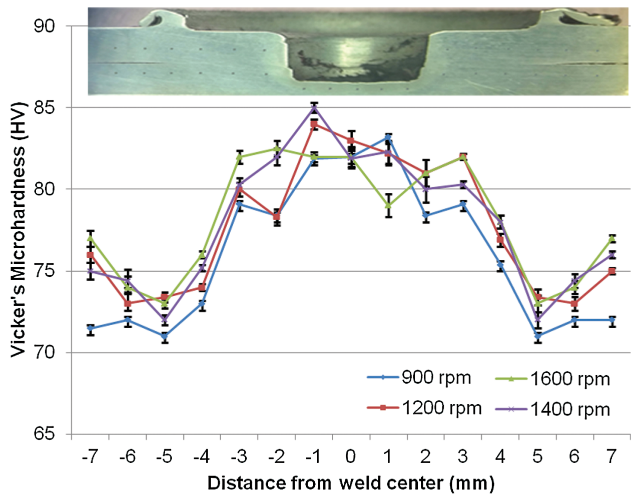

Fig. 10. Microhardness distribution of conventional FSSW joints across weld cross-section.

the additional stirring action by the tool after plunging. It caused the increase in material flow and increased overall bonding area of the joints. It is also observed that the change in tool rotational speed has a significant effect on lap shear strength, irrespective of the method used. The highest lap shear strength of 3.54 kN and 5.31 kN are recorded in conventional (1600 rpm) and swept FSSW (1400 rpm) processes, respectively.

In conventional FSSW, the lap shear strength is linearly improved with the tool rotational speed. But in swept FSSW, the lap shear strength is found to continuously increase up to the tool rotational speed of 1400 rpm. Further increase in the tool rotational speed to 1600 rpm decreased the lap shear strength. This could be due to insufficient friction between base metal and tool in the higher tool rotational speed, which could affect the material flow in weld zone and result in low strength. The high tool rotational speed may cause high heat and inertial force

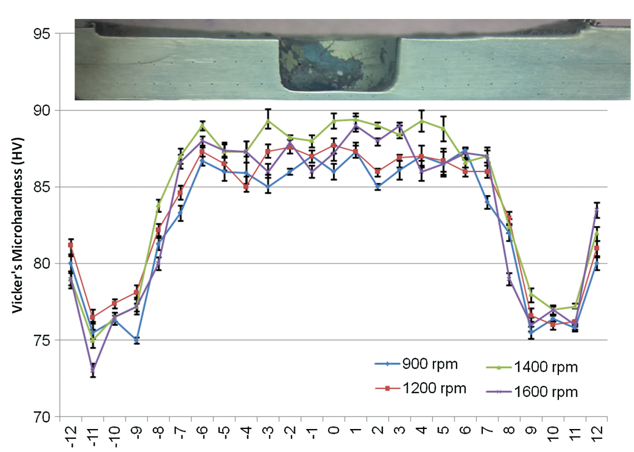

Fig. 11. Microhardness distribution of swept FSSW joints across weld cross-section.

that could also affect the weld strength [27]. Irrespective of a tool rotational speed, the lap shear strength increased by 35% to 46% in swept FSSW joints as compared to the conventional FSSW joints. Hence, according to the results, the size of the weld area significantly influence the overall increase in lap shear strength of AA6061-T6 swept FSSW joints.

The lap shear strength of conventional and swept FSSW samples was further applied in Analysis of variance (ANOVA) to ensure the significance of the results. The values such as F, F_{critical} and p were computed for the experimentally measured results. If the computed F value is not larger than F_{critical} value, it implies that there is a significant difference between the measured data. The value of p is the probability of obtaining significant difference from the observed F value. If the p-value is quite small (much lower than 0.05), it implies that the chosen parameters have significant effect on the response variable [28, 29]. From the current ANOVA analysis, p is computed to be 0.046, which reveals that rotational speeds have a significant effect on lap shear strength. Furthermore, $F = 47.56$ is found to be greater than $F_{\text{critical}} = 5.987$, which regards that there is a significant difference in the results of swept FSSW and conventional FSSW.

3.5. Microstructural Study

The cross-sectional macroscopic appearance and the microscopic structure of different zones made by a conventional FSSW and swept FSSW at the speed of 1400 rpm are shown in Figures 13 and 14, respectively. In both the methods of FSSW, the SZ followed by TMAZ have finer grains as compared with the BM. This is because of the stirring action of the weld tool and dynamic recrystallization associated with the process. The grains in the SZ of swept FSSW are characterized by finer grains compared to the conventional FSSW, which can be the extra heat generation during the additional stirring action of the tool which is inline with the effect reported by Venukumar et al. [11].

3.6. Fracture Morphologyunder Lap-Shear Loading

Shear mode of fracture, nugget pullout mode of fracture and circumferential mode of fracture were observed from the appearance of fracture surfaces under the lap shear loading as shown in Figures 15 and 16.

While studying at the fracture surfaces from conventional FSSW samples (as shown in Fig. 15), shear mode of fracture is observed in the sample prepared by the rotational speed of 900 rpm. The crack growth provoked around the keyhole and showed the low shear strength. Nugget pullout mode of fracture is observed in the samples prepared at the rotational speed of 1200 and 1400 rpm. It is observed that the bonding area between the lower and upper sheet was sheared off, and led to the fracture in the

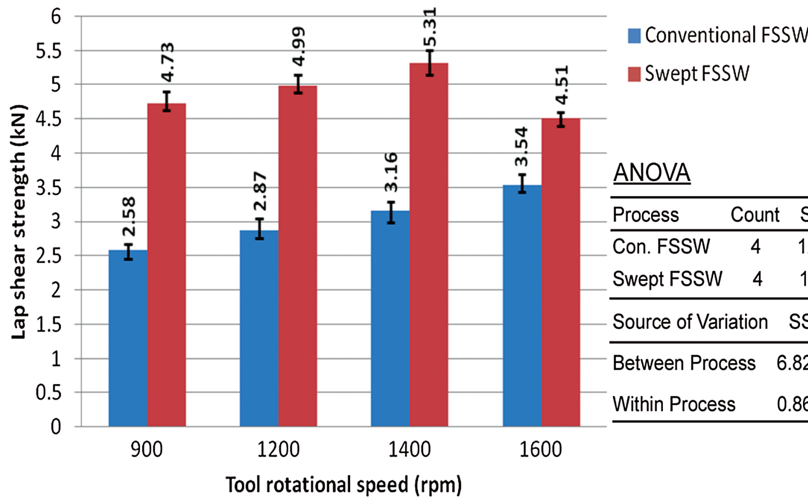

ANOVA

Process	Count	Sum	Average	Variance
Con. FSSW	4	12.15	3.037	0.1682
Swept FSSW	4	19.54	4.885	0.1187

Source of Variation	SS	DF	MS	F	P-Value	F-crit
Between Process	6.826	1	6.82	47.56	0.00046	5.987
Within Process	0.861	6	0.143			

Fig. 12. Comparison of lap shear strength between conventional and swept FSSW with ANOVA statistical analysis.

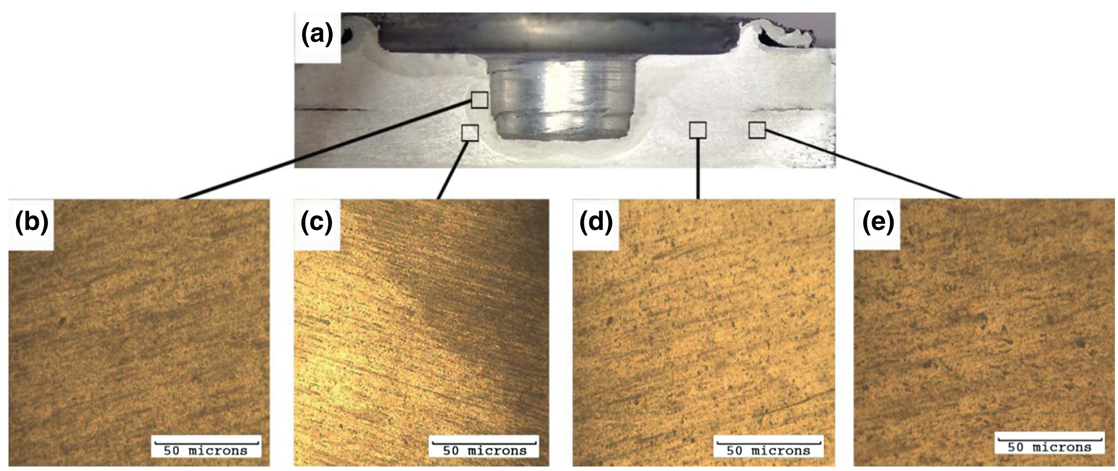

Fig. 13. The microstructure of cross-section of the weld made by conventional FSSW at the tool rotational speed of 1400 rpm: (a) Macrograph showing various zones, (b) SZ, (c) SZ-TMAZ interface, (d) HAZ, (e) BM.

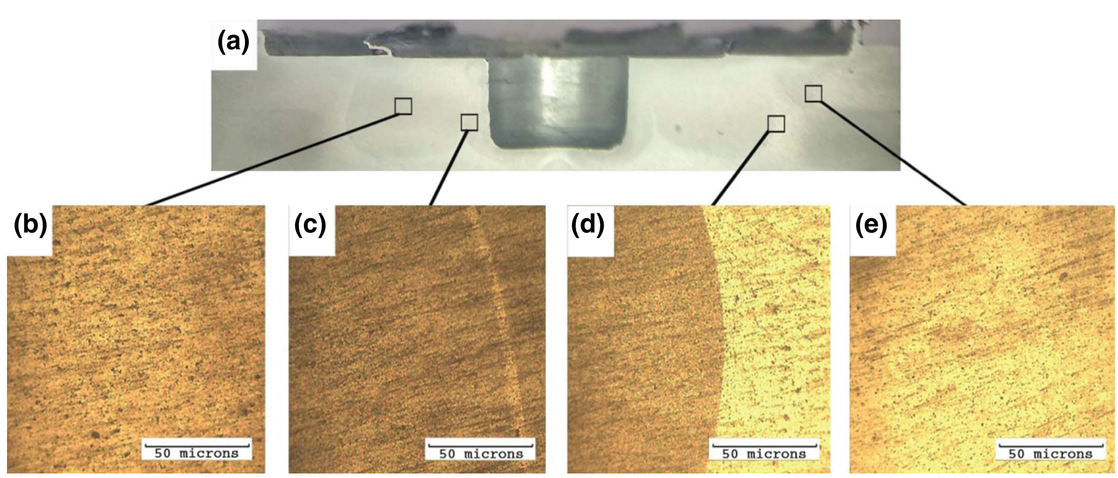

Fig. 14. The microstructure of cross-section of the weld made by swept FSSW at the tool rotational speed of 1400 rpm: (a) Macrograph showing various zones, (b, c) SZ, (d) SZ-TMAZ Interface, (e) HAZ.

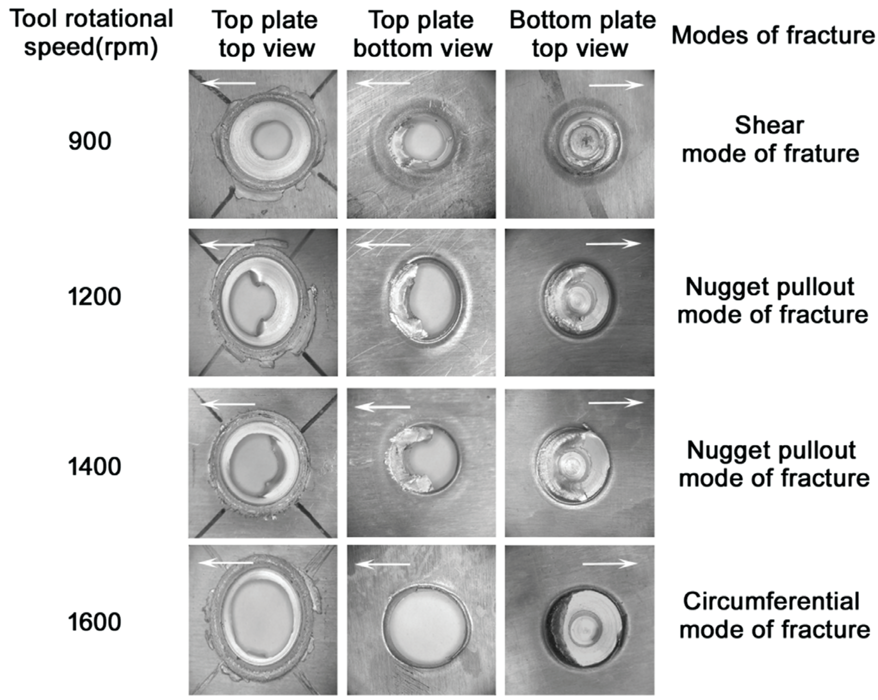

Fig. 15. Photograph showing fracture surfaces of lap shear tested specimen of conventional FSSW.

nugget [30]. It is further noted that the partial amount of nugget is placed on the sheared top plate. The circumferential mode fracture is observed in the sample made at the tool rotational speed of 1600 rpm.

Regarding swept FSSW samples, the circumferential mode fracture is observed irrespective of the rotational speed (as shown in Fig. 16). The circumferential mode of fracture is noticed in weld joints of maximum lap

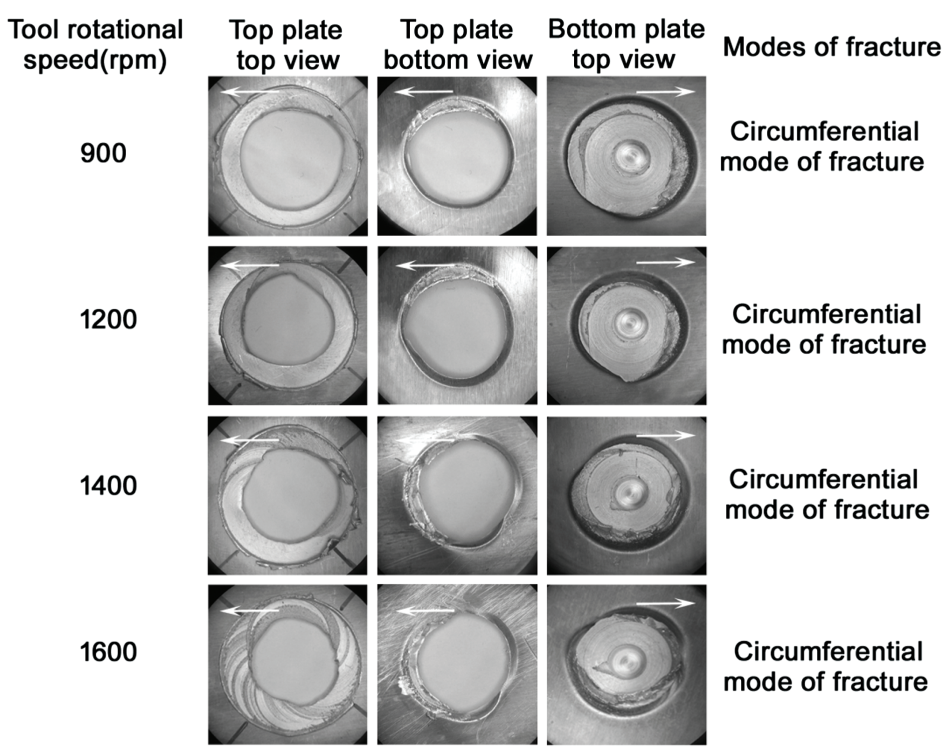

Fig. 16. Photograph showing fracture surfaces of lap shear tested specimen of swept FSSW.

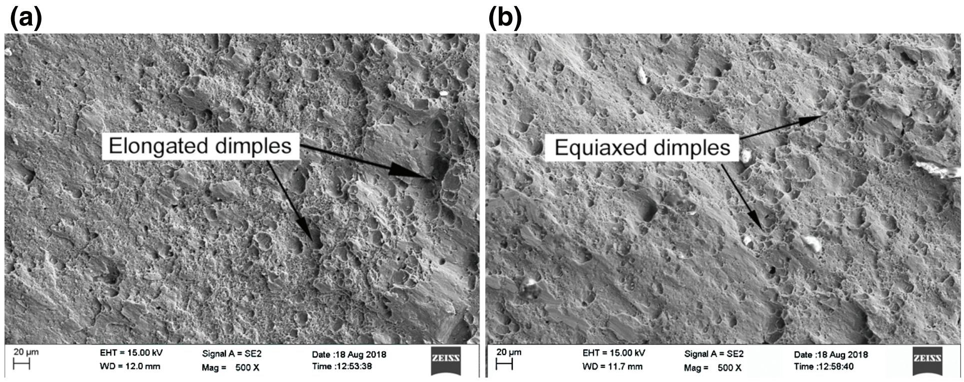

Fig. 17. FESEM fractography of the welded joints produced by (a) conventional FSSW and (b) swept FSSW.

shear strength, irrespective of FSSW method used. This is worth notable point that inline with the report published by Venukumar et al. [12].

Figure 17 shows FESEM fractography of SZ of broken lap-shear specimen that was prepared at 1400 rpm. The presence of elongated dimples in the direction of applied load are observed, which is usually characterized by the ductile fracture of the joint [31]. The fracture surface of conventional FSSW joint (Fig. 17(a)) shows the various sizes of well-elongated dimples. The swept FSSW joint (Fig. 17(b)) showed a large number of fine and equiaxed dimples, which imply the enhanced bonding and higher joint strength.

4. CONCLUSIONS

The conventional and swept FSSW on 6061-T6 aluminium alloy at different tool rotational speeds were done and the mechanical properties, microstructure and fracture behaviour of the weld zones were studied. The following conclusions are drawn based on the results obtained:

- Swept FSSW joints have shown considerably higher lap shear strength and hardness values than conventional FSSW joints. The increase in lap shear strength in swept FSSW is due to the additional stirring action of the tool that leads to a larger bonding area. The results showed that the compelling increases in the weld area as swept FSSW influences the higher strength of the joint.
- The weld samples under the swept FSSW at the tool rotational speed of 1400 rpm exhibited the maximum lap shear strength of 5.31 kN. Also noted that the further increase of tool rotational speed beyond 1400 rpm affects the mechanical properties.
- Both the conventional and swept FSSW processes show finer grains in SZ and TMAZ due to dynamic recrystallization. But the grain size of the SZ in the swept FSSW joints is found to be smaller than the conventional FSSW joints.
- Shear fracture, nugget pullout fracture and circumferential mode of fracture were observed in conventional FSSW samples at different tool rotational speeds, whereas only circumferential mode of fracture was observed in swept FSSW samples.

References and Notes

1. Stojanovic, B., Bukvic, M. and Epler, I., **2018**. Application of aluminum and aluminum alloys in engineering. *Applied Engineering Letters, 3*(2), pp.52–62.
2. Prakash, S., Sasikumar, R. and Elango Natarajan, **2018**. Superior material properties of hybrid filler-reinforced aluminum MMC through double layer feeding technique adopted in bottom tapping stir casting. *High Temperature Material Processes, 22*, pp.249–258.
3. Balaguru, S., Navin Kumar, K. and Elango Natarajan, **2018**. Experimental and numerical investigation on mechanical properties of AA6061T6 reinforced with SiC and Al_2O_3. *International Journal of Mechanical and Production Engineering Research and Development*, (Special Issue), pp.201–206.
4. Benedyk, J.C., **2010**. Aluminum alloys for lightweight automotive structures. in *Materials, Design and Manufacturing for Lightweight Vehicles*. Woodhead Publishing, Chap. 3, pp.79–113, DOI: 10.1533/9781845697822.1.79.
5. Hancock, R., **2004**. Friction welding of aluminum cuts energy cost by 99%. *Welding Journal, 83*, pp.40–43.
6. Su, P., Gerlich, S., North, T.H. and Bendzsak, G.J., **2006**. Energy utilisation and generation during friction stir spot welding. *Science and Technology of Welding & Joining*, *11*, pp.163–169.
7. Rajan, R., Kah, P., Mvola, B. and Martikainen, J., **2016**. Trends in aluminium alloy development and their joining methods. *Reviews on Advanced Materials Science, 44*, pp.383–397.
8. Ojo, O.O., Taban, E. and Kaluc, E., **2015**. Friction stir spot welding of aluminum alloys: A recent review. *Materials Testing*, *57*, pp.609–627.
9. Lee, S.H., Lee, D.M. and Lee, K.S., **2017**. Process optimisation and microstructural evolution of friction stir spot-welded Al6061 joints. *Materials Science and Technology*, *33*, pp.719–730.
10. Suresh, S., Venkatesan, K. and Elango Natarajan, **2018**. Influence of SiC nanoparticle reinforcement on FSS welded 6061-T6 aluminum alloy. *Journal of Nanomaterials, 2018*, pp.1–10, DOI: 10.1155/2018/7031867.
11. Venukumar, S., Babya, B., Muthukumaran, S. and Satish, K., **2014**. Microstructural and mechanical properties of walking friction stir spot welded AA6061-T6 sheets. *Procedia Materials Science*, *6*, pp.656–665.
12. Venukumar, S. and Muthukumara, S., **2014**. Failure modes and fatigue behavior of conventional and refilled friction stir spot welds in AA6061-T6 sheets. *International Journal of Fatigue, 61*, pp.93–100.

13. Venukumar, S., Yalagi, S. and Muthukumaran, S., **2013**. Comparison of microstructure and mechanical properties of conventional and refilled friction stir spot welds in AA6061-T6 using filler plate. *Transactions of Nonferrous Metals Society of China*, *23*, pp.2833–2842.
14. Cox, C.D., Gibson, B.T., Strauss, A.M. and Cook, G.E., **2012**. Effect of pin length and rotation rate on the tensile strength of a friction stir spot-welded Al alloy: A contribution to automated production. *Materials and Manufacturing Processes, 27*, pp.472–478.
15. Karthikeyan, R. and Balasubramanian, V., **2012**. Optimisation and sensitivity analysis of friction stir spot-welding process parameters for joining AA6061 aluminum alloy. *International Journal of Manufacturing Research, 7*, pp.257–272.
16. Okamoto, K., Hunt, F. and Hirano, S., **2005**. Development of friction stir welding technique and machine for aluminum sheet metal assembly-friction stir welding of aluminum for automotive applications (2); SAE Technical paper 2005-01-1254. DOI: 10.4271/2005-01-1254.
17. Awang, M., Ismail, A. and Zaman, M.A.K., **2016**. Effect of process parameters on the strength of swept friction stir spot welded plates. *Machining Joining and Modifications of Advanced Materials, Advanced Structured Materials*. Singapore, Springer. pp.105–110.
18. Brown, J., Burford, D.A., Widener, C.A., Horn, W., Talia, J. and Tweedy, B.M., **2009**. Corrosion and fatigue evaluation of swept friction stir spot welding through sealants and surface treatments. *Friction Stir Welding & Processing V*, San Francisco, California. pp.273–285.
19. Su, Z.M., He, R.Y., Lin, P.C. and Dong, K., **2016**. Fatigue of alclad AA2024-T3 swept friction stir spot welds in cross-tension specimens. *Journal of Materials Processing Technology, 236*, pp.162–175.
20. Su, Z.M., He, R.Y., Lin, P.C. and Dong, K., **2014**. Fatigue analyses for swept friction stir spot welds in lap-shear specimens of alclad 2024-T3 aluminum sheets. *International Journal of Fatigue, 61*, pp.129–140.
21. Buffa, G., Fratini, L. and Piacentini, M., **2008**. On the influence of tool path in friction stir spot welding of aluminum alloys. *Journal of Materials Processing Technology, 208*, pp.309–317.
22. Awang, M., Ahmat, I.M. and Hussain, P., **2011**. Experience on friction stir welding and friction stir spot welding at universiti teknologi petronas. *Journal of Applied Sciences, 11*, pp.1959–1965.
23. Addison, A.C. and Robelou, A.J., **2004**. Friction Stir Spot Welding: Principal Parameters and Their Effects. *Proceedings of the 5th International Conference on Friction Stir Welding*, Metz, France.
24. Yin, Y.H., Ikuta, A. and North, T.H., **2010**. Microstructural features and mechanical properties of AM60 and AZ31 friction stir spot welds. *Materials and Design, 31*, pp.4764–4776.
25. Liu, H., Zhang, H., Pan, Q. and Yu, L., **2012**. Effect of friction stir welding parameters on microstructural characteristic and mechanical properties of 2216-T6 aluminium alloy joints. *International Journal of Material Forming*, *5*, pp.235–241.
26. Zhang, Z., Yang, X., Zhang, J., Zhou, G., Xu, X. and Zou, B., **2011**. Effect of welding parameters on microstructure and mechanical properties of friction stir spot welded 5052 aluminum alloy. *Materials & Design, 32*, pp.4461–4470.
27. Saeid, H.D., Taher, A., Samrand, R.A. and Arvin, B., **2013**. Friction stir spot welding of dissimilar polymethyl methacrylate and acrylonitrile butadiene styrene sheets. *Materials & Design, 45*, pp.135–141.
28. Sathiyamoorthy, V., Sekar, T. and Elango, N., **2015**. Optimization of processing parameters in ECM of die tool steel using nanofluid by multiobjective genetic algorithm. *Scientific World Journal, 2015*, pp.1–6. DOI: 10.1155/2015/895696.
29. Natarajan, E., Kaviarasan, V., Lim, W.H., Tiang, S.S. and Tan, T.H., **2018**. Enhanced multi-objective teaching-learning-based optimization for machining of delrin. *IEEE Access, 6*, pp.51528–51546. DOI: 10.1109/ACCESS.2018.2869040.
30. Suresh, S., Venkatesan, K. and Rajesh, S., **2019**. Optimization of Process Parameters for Friction Stir Spot Welding of AA6061/Al_2O_3 by Taguchi Method. *AIP Conference Proceedings*, Vol. 2128, p.030018, DOI: 10.1063/1.5117961.
31. Mazzaferro, C.C.P., Rosendo, T.S., Tier, M.A.D., Mazzaferro, J.A.E., Dos Santos, J.F. and Strohaecker, T.R., **2015**. Microstructural and mechanical observations of a galvanized TRIP steel after friction stir spot welding. *Materials and Manufacturing Processes, 30*, pp.1090–1103.

Received: 6 February 2019. Accepted: 30 August 2019.